Phase Diagram, Melt Growth and Characterization of $Cd_{0.8}Zn_{0.2}Te$ Crystals for X-Ray Detector

Ching-Hua Su

Materials and Processing Laboratory, Engineering Directorate, EM31 NASA/Marshall Space Flight Center, Huntsville, Alabama 35812 USA, E-mail address: ching.h.su@nasa.gov Tel: (256)544-7776

Abstract

In this study, the solidus curve of the $Cd_{0.8}Zn_{0.2}Te$ homogeneity range was constructed from the partial pressure measurements by optical absorption technique which provided the information of the melt growth parameters to process crystals with the required electrical resistivity. The melt growth of $Cd_{0.8}Zn_{0.2}Te$ crystals were then processed by directional solidification under controlled Cd overpressure. During the growth experiments, several procedures have been developed to improve the crystalline quality: (1) minimizing the contamination of impurities (2) improving the structural defects and (3) minimizing the Te-precipitates within the grown crystals to enhance charge transport properties. Additionally, the thermal conductivity, electrical conductivity, and Seebeck coefficient of a vapor-grown CdTe and two melt-grown $Cd_{0.8}Zn_{0.2}Te$ crystals were measured between 190°C and 780°C to provide an in-depth understanding of the thermal and electrical conduction mechanisms of the crystals as well as the prospect of its thermoelectric applications.

Keywords: Phase diagram; $Cd_{0.8}Zn_{0.2}Te$ crystals; Directional solidification; Controlled overpressure

1. Introduction

In the application of room temperature high-energy radiation detector, there are two critical requirements for the detecting semiconductor such as CdZnTe [1-4]. The first one is high electrical resistivity, greater than 10^9 Ω-cm, to reduce the bulk leakage current. This requirement can only be met with materials of low carrier concentrations which are controlled by the concentrations of intrinsic defects, i.e., native point defects such as Cd vacancy, and extrinsic point defects, including intentional and unintentional dopants. The information on the solidus curve and the equilibrium vapor pressures over this narrow homogeneity range ternary compound is therefore an important database in the control of the concentration of native point defects. The other critical requirement is the reduction of structural defects which act as trapping and recombination centers. Various defects that have been shown to adversely affect charge transport in CdZnTe [5,6] are grain boundaries, twins, Te inclusions, dislocations, and subgrain boundaries. [7]. Due to the strong trapping at grain boundaries, high-performance radiation detectors are almost exclusively fabricated from CdZnTe single crystals. Even so, defects within the single crystals such as Te precipitates/inclusions [8], subgrain boundaries, slip planes and dislocation can also cause charge transport problems. In this case, the knowledge of homogeneity range is also important in that the solid solubility limit determines the boundary of the formation of Te-rich precipitates during the grown crystals.

The solidus curve delineates the solubility of group II or VI elements in the II-VI compound and the existence of homogeneity range is material's nature to reduce the Gibbs energy of formation by increasing its entropy term [9]. Therefore, the solubility, i.e., the maximum amount of solute can be incorporated into solid compound, is zero both at temperature

of absolute zero and at the maximum melting temperature (due to the phase transition). Along the temperatures in-between, the solubility goes through a maximum as a function of temperature, known as retrograde solubility. The maximum non-stoichiometry was estimated for the $Cd_{1-x}Zn_xTe$ solid solutions, for $x \leq 0.15$, based on the projection of the pressure-temperature diagram [10-12] and it was found that the $Cd_{1-x}Zn_xTe$ solidus gradually shifts towards Te-rich side with increasing ZnTe content, x. With most of the studies focusing on the processing of CdTe and $Cd_{0.9}Zn_{0.1}Te$ crystals by melt growth techniques, such as vertical gradient freeze (VGF) [13], high pressure Bridgman (HPB) [6,7] and traveling heater method (THM) [14] for the application of X-ray detectors [15], it is worthwhile to investigate other composition of the pseudo-binary, such as $Cd_{0.8}Zn_{0.2}Te$ which has been grown by traditional vertical Bridgman but needed improvements in several areas as compared to $Cd_{0.85}Zn_{0.15}Te$ [16]. Additionally, the higher energy bandgap of $Cd_{0.8}Zn_{0.2}Te$ increases the maximum achievable electrical resistivity than that of $Cd_{0.9}Zn_{0.1}Te$. The extra Zn also promotes solution hardening which helps to reduce the dislocation density. In this study, the solidus curve of $Cd_{0.8}Zn_{0.2}Te$ was determined from the partial pressure measurements by optical absorption technique which provided the information for the melt growth parameters to process crystals with the required electrical resistivity.

During the practice of melt growth experiments, several procedures have been developed to improve the crystalline quality by minimizing the contamination of impurities as well as improving the structural defects within the grown crystals to enhance charge transport properties. These procedures are listed briefly below and will be given in detail later.

- A procedure was developed to homogenize pure elements through localized eutectic reaction using traveling zone process.

- The Cu and other elemental contaminations were minimized by homogenizing the CdZnTe ampoule under external vacuum condition.
- The internal surface of the empty growth ampoule was etched by HF before the loading of starting material to reduce the interaction between sample and fused silica ampoule during growth.
- By controlling the Cd overpressure during growth, high resistivity CdZnTe crystals have been consistently grown with the In dopant concentration of 4 to 6 ppm, atomic.
- A mechanical pulsed perturbation was applied to growth ampoule during the nucleation stage of crystal to promote the yield of single crystal.
- An optimal temperature for Cd reservoir was established to minimize the density of Te inclusions.
- A cooling schedule of Cd reservoir temperature during and after the growth process was developed to improve the radial uniformity of electrical properties in the grown crystal.

2. Phase Diagram of $Cd_{0.80}Zn_{0.20}Te$ Solid Solution

The data on the composition – temperature – partial pressures (x_{Te}–T – P_{Te2}), corresponding to the Te-saturated CdTe solid, have been established by the partial pressure measurements using the optical absorption method [17]. Recently, the same method has been conducted for the pseudo-binary of $Cd_{0.80}Zn_{0.20}Te$ [18]. Four samples with known masses of Cd, Zn and Te were reacted in fused silica optical cells of known volume profile. The partial pressures of Te_2 and Cd, in equilibrium with the samples between 485 and 1160°C, were determined by measuring the optical density of the vapor phase from the ultra-violet to the

visible range. The composition of the condensed phase or phases was then calculated from the original masses and the amount of material in the vapor phase to establish the corresponding x_{Te} – T – P_{Te_2} data, including five Te-rich solidus points.

The detailed description of the experimental setup and procedures has been presented in Ref.[18]. A brief summary is given here. The T-shaped optical cells were made of fused silica. The top of the T-shaped cell consisted of an 18 mm OD, 15 mm ID cylindrical tube with flat, parallel quartz windows at both ends. The optical path length is either 10 or 5 cm. The bottom of the T-cell was a sidearm made by attaching a 6 cm long, 12 mm OD, 8 mm ID tube to the midpoint of the cell-proper, referred to as stem, which was joined coaxially by a 10 cm long 18 mm OD, 15 mm ID tube referred to as reservoir. The volumes of the empty cells were measured as a function along the length of the cell by adding distilled water. The cells were cleaned and then baked at 1180 ^{o}C for 18 h under vacuum.

The starting elemental materials were 99.9999% purity Cd rod, Te bar and Zn teardrops. The elements were weighed by a Mettler AT-201 balance, with a resolution of 10 μg, except for CZT-1, which was weighed by a Chyo Jupiter M1-20 microbalance with resolution of 1 μg. Four CdZnTe cells, CZT-1 to -4 and a calibration cell each for the Cd and Te element, as listed in Table 1, were prepared. The weighed elements were loaded directly into the baked-out optical cells, which were sealed off at a vacuum level less than $2x10^{-8}$ atm. The sealed cells were placed inside a five-zone T-shaped furnace. The furnace with the optical cell inside was then placed in a double-beam reversed-optics spectrophotometer (OLIS Inc., model 14H) with the optical cell proper in the path of the sample beam, and the reference beam passed under the furnace. The optical density, defined as $D = \log_{10}(I_{reference}/I_{sample})$, where I is the intensity (of reference or sample beam), was measured between the wavelengths of 200 and 700 nm. The light source was

a deuterium lamp for wavelengths below 275 nm and a Xenon lamp for wavelengths above 275 nm. The typical instrument band pass was 0.2, 1.2, and 2.7 nm, respectively at the wavelengths of 600, 290, and 200 nm. The temperature of the optical cell-proper, $T_{O.C.}$, was kept at 1050, 1100 or 1150 $\pm$ 2ºC while the temperatures of the stem and the reservoir sections decreasing monotonically to T_R, i.e., the temperature of the reservoir for the sample. A baseline spectrum was measured first for each $T_{O.C.}$ with the reservoir temperature below 400ºC.

Table 1. The sample name, optical path length, the total mass and atomic fractions of Zn, x_{Zn}, and Te, x_{Te} of each optical cell.

Sample	Optical path (cm)	Total mass (g)	x_{Zn}	x_{Te}
CZT-1	9.83	20.539284	0.099954	0.500206
CZT-2	9.90	20.84812	0.099917	0.500494
CZT-3	9.90	20.50930	0.099995	0.500015
CZT-4	5.00	20.47089	0.100016	0.499990
Cd	9.90	2.1345	0	0
Te	9.90	3.316	0	1.0

The typical spectra of optical density vs. wavelength on a CZT sample for a series of runs with increasing sample temperatures is presented in Figure 1, which shows the absorption peak of Cd atom at 228.7 nm and a series of vibronic absorption peaks from diatomic Te molecule, Te_2, between 350 and 550 nm. The partial pressures of Te_2, P_2, and Cd, P_{Cd}, were derived as the followings. First, the partial pressure of Te_2 was determined from the measured optical density using the calibration constants from a pure Te cell between 400 and 600 nm. Usually, the pressure was taken as the average of the values measured at 4 to 6 wavelengths where the optical density was between 0.1 and 2.5 with the upper limit being 3.0 for the detector. To calculate the partial pressure of Cd, the measured optical density in the UV region was assumed to be the result of a linear superposition of Cd and Te_2 absorption. The contribution of Te_2 to the optical

density in the UV region was calculated from the measured Te_2 partial pressure and the calibration constants of pure Te. This contribution was subtracted from the measured optical density and the partial pressure of Cd, P_{Cd}, was calculated from the remained optical density using the calibration results from an optical cell of pure Cd.

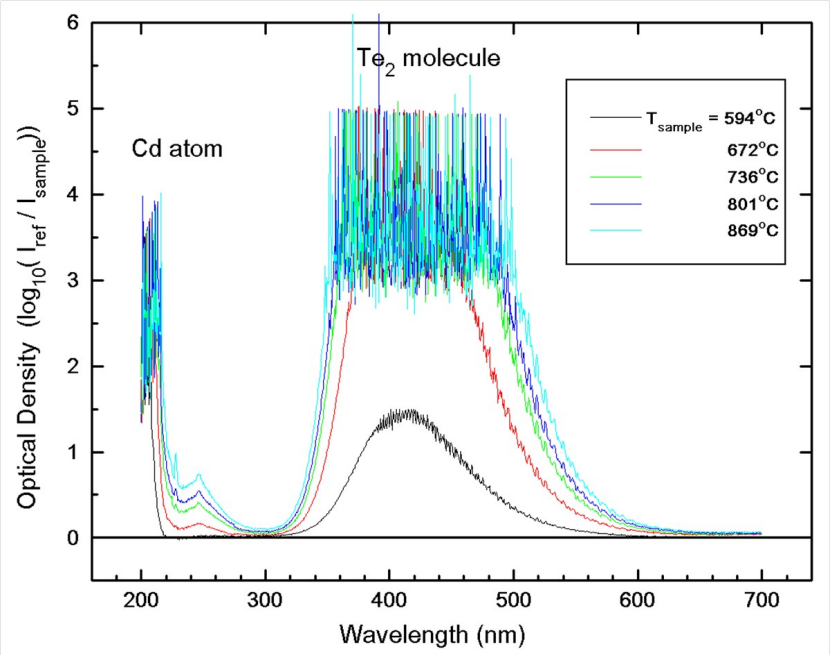

Figure 1. Five spectra of optical density vs. wavelength for a CZT sample from a series of runs with different sample temperatures show the absorption of Cd atom at 228.7 nm and a series of vibronic absorption peaks from diatomic Te molecule, Te_2, between 350 and 550 nm.

The measured values of P_2 for all of the four CZT runs, together with the pressure over pure Te, P_2^o, are plotted against 1000/T (T is T_R in K) in Figures 2(a). The measured P_2 shows that, for CZT-1, 2 and 3, the samples started out as Te-saturated at low temperature. As the temperature increased, sample CZT-1 and 3 moved into the homogeneity range as the measured P_2 started to flatten out and, eventually, joined the Te-saturated loop at a higher temperature. For CZT-2, the sample composition remained Te-saturated as the measured P_2 followed the so-called

three-phase loop throughout most of the measuring temperatures. For CZT-4, only high temperature measurements were performed and the data show that the sample composition was inside the homogeneity range at the low end of the measured temperatures and moved onto the Te-saturated loop at a higher temperature. The compositions of CZT-1, 2 and 3 were initially inside the two-phase field of Te-rich $Cd_{0.80}Zn_{0.20}Te$ (s) + Te-rich melt, and this condition remained for CZT-2 throughout the runs. As the temperature and the equilibrium P_2 increased, samples CZT-1 and 3 were losing Te to the vapor phase faster than the other two components. Therefore, their compositions became progressively less Te-rich and moved inside the homogeneity range of $Cd_{0.80}Zn_{0.20}Te$ solid. As the temperature kept increasing, the measure P_2 flattened inside the homogeneity range as the partial pressure of the group II components kept on increasing. The sample composition eventually started to move back toward the Te-rich direction and finally crossed the Te-rich homogeneity range and became a mixture of Te-rich $Cd_{0.80}Zn_{0.20}Te$ (s) + Te-rich melt again. Sample CZT-4 started inside the homogeneity range and crossed the solidus temperature into the Te-rich mixture as the temperature increased. As the temperature further increased, the measured P_2 for all samples decreased rapidly following the three-phase loop. At even higher temperature, all four samples broke away from the three-phase loop, and the measured P_2 flattened as the temperature increased. Supposedly, the break point temperature should be close to the liquidus temperature of the non-stoichiometric $Cd_{0.80}Zn_{0.20}Te$ samples with the Te content higher than 0.50.

The measured P_{Cd} for all four samples are shown in Figure 2(b) together with P_{Cd} over pure Cd element, P^o_{Cd}. The data are consistent with the P_2 shown in Figures 2(a) in that all samples went through the homogeneity range except CZT-2, which was Te-saturated throughout the runs. As shown in Figure 2(b), the small variation in the sample compositions didn't affect

the measured P_{Cd} in the melt as much as the large differences in the measured P_{Cd} over the homogeneity range of the solid. For the growth condition of directional solidification, to be described in detail later, the melt was maintained at a temperature of 1145±5°C and the measured P_{Cd} in equilibrium with the melt at this temperature, 1.8 atm, can be provided by a pure Cd reservoir at 820°C with the Cd pressure over pure Cd, P^{o}_{Cd}, expressing as a function of temperature by [19]:

$$\log_{10} P^{o}_{Cd}(atm) = -5{,}317/T(K) + 5.119 \qquad \text{Eq. (1)}$$

Assuming the vapor phase is ideal, the Gibbs energy of formation of CdTe in $Cd_{0.80}Zn_{0.20}Te$(s) from Cd(g) and Te_2(g) at 1atm was calculated from the measured P_{Cd} and P_2 for the data points inside the homogeneity range as well as on the three-phase loop and they can be fitted using the equation [18]:

$$\Delta G_{f,CdTe}(x=0.20) = RT\ln\left(P_{Cd}P_{Te_2}^{1/2}\right) = -68{,}642 + 44.4956T \quad \text{(cal/mole)} \qquad \text{Eq. (2)},$$

where R is gas constant and T in K. Using Eq. (1), the Cd partial pressure for the Te-saturated section of $Cd_{0.80}Zn_{0.20}Te$(s) was calculated from the corresponding measured P_2 and is plotted in Figure 2(b) as the lower dotted line which is consistent with the measured P_{Cd}.

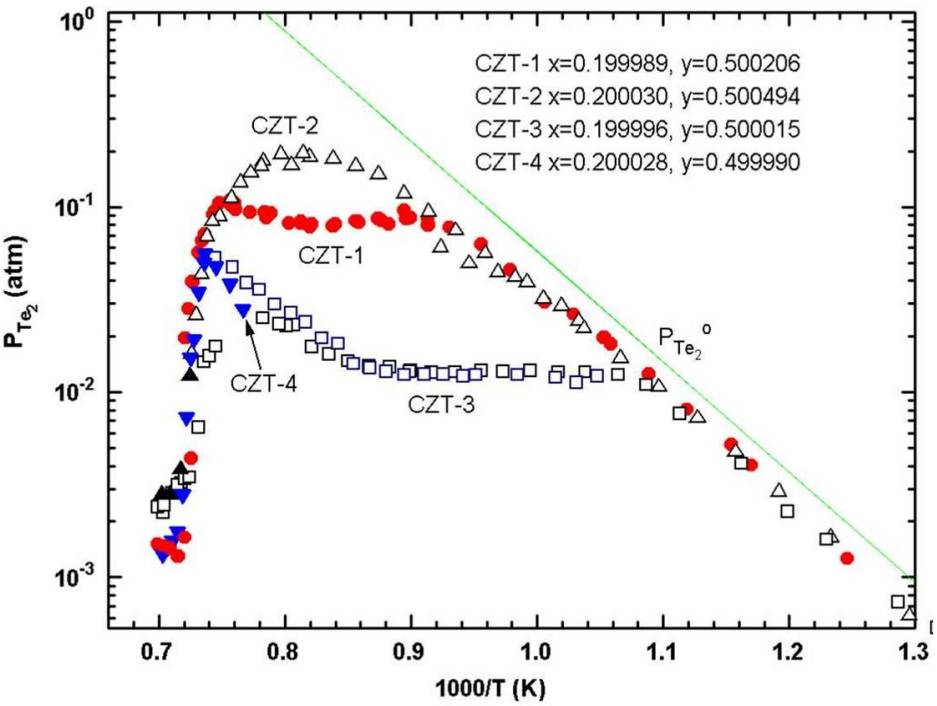
CZT-1 x=0.199989, y=0.500206
CZT-2 x=0.200030, y=0.500494
CZT-3 x=0.199996, y=0.500015
CZT-4 x=0.200028, y=0.499990
CZT-2
CZT-1
CZT-4
CZT-3
$P_{Te_2}^{o}$
P_{Te_2} (atm)
1000/T (K)

(a)

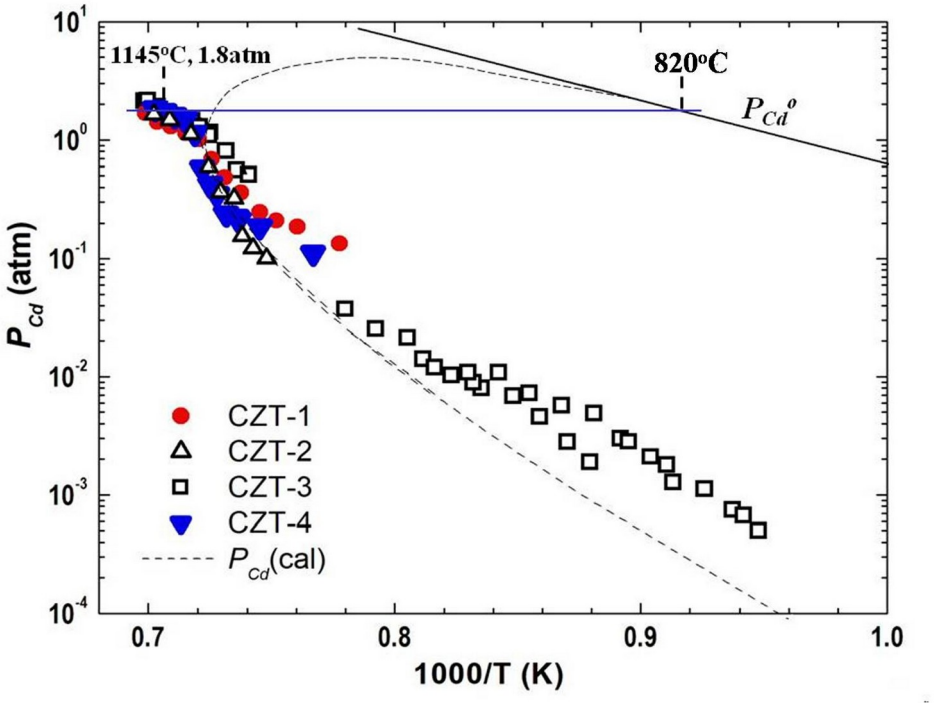
1145°C, 1.8atm
820°C
P_{Cd}^{o}
CZT-1
CZT-2
CZT-3
CZT-4
P_{Cd}(cal)
P_{Cd} (atm)
1000/T (K)

(b)

Figure 2. Measured partial pressures of Te_2 (a) and Cd (b) for 4 samples of $(Cd_{1-x}Zn_x)_{1-y}Te_y$ with the initial values of x and y given in (a). The upper dashed curve in (b) is the approximated P_{Cd} for the Cd-saturated condition (taken from Figure 3 in Ref.[18]).

The partial pressure of Zn were then derived from the Gibbs energy of formation of ZnTe in $Cd_{0.80}Zn_{0.20}Te$(s) which was approximated from the best fit quasi-regular interaction parameters determined in Ref. [19] for the CdTe-ZnTe solid solution. As the temperature increased the composition of the condensed phase, or phases, in equilibrium with the partial pressures changed because of the incongruent sublimation of the sample. Assuming that the gas phase is ideal, the masses of Cd, Zn and Te in the vapor phase can be calculated from their partial pressures and the measured volume and temperature profiles for each data point [18]. By subtracting the mass of each element in the vapor phase from the original masses, the composition of the solid sample at each data point can be calculated and is shown in Figure 3. The solidus curve on the Te-rich side of the homogeneity range gives the estimated maximum limit to be x_{Te} = 0.50012 at 977 °C.

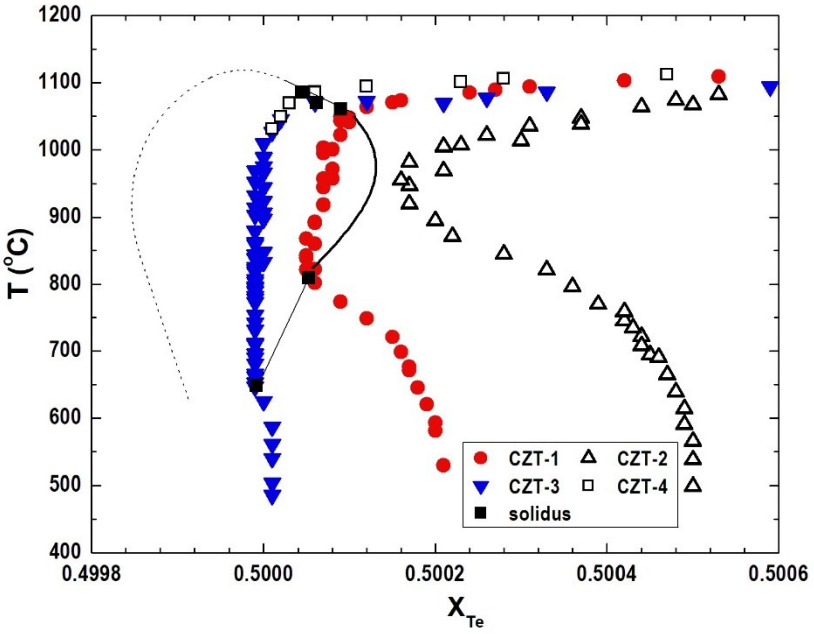

Figure 3. The sample composition, x_{Te}, calculated from each partial pressure data point and the five solidus points, shown as solid black squares, determined from these data. The maximum limit is estimated to be $x_{Te} = 0.50012$ at 977 °C. The dotted curve on the Cd-rich region is arbitrarily drawn (taken from Figure 7 in Ref.[18]).

3. Procedures to Improve Quality of Melt Grown CdZnTe Crystals

3.1 Melt Growth under Controlled Cd Overpressure

The conditions for the growth of inclusion-free CdZnTe single crystals have been previously investigated. In the vertical gradient freeze growth of $Cd_{1-x}Zn_xTe$ (x = 0.04) as the lattice matched substrate for the epitaxial growth of HgCdTe IR detectors, the Cd pressure at the congruent melting point was estimated and the corresponding amounts of Cd were added to the ampoules to reach 1 to 1.3 atm of Cd [20]. Asahi et al. [21] and Koyama et al. [22] have grown $Cd_{1-x}Zn_xTe$ (x = 0.03 – 0.04) by VGF under a Cd overpressure to minimize the size of precipitates in the grown crystals. Szeles et al. [23,24] have grown semi-insulating $Cd_{0.9}Zn_{0.1}Te$ crystals for the room-temperature x- and gamma-ray radiation detectors using an electro-dynamic gradient technique with a controlled Cd overpressure.

Under the crystal growth environments, to be presented later, the partial pressures of Te_2 and Cd over the melt at 1145°C differ by 3 orders of magnitude. During the crystal growth of CdZnTe by directional solidification, a starting material of stoichiometric composition, i.e., x_{Te} = 0.5000, will lose more Cd to the vapor phase than Te, and the composition of the condensed phase will shift toward the Te-richer direction. The amount of this shift depends on the total sample mass, the temperature and volume profiles. There are two consequences the shift creates: (1) Cd vacancy and (2) Te-rich second phase. Based on a defect chemistry analysis to interpret the $x_{Te} - T - P_{Te_2}$ data for $Cd_{0.8}Zn_{0.2}Te$, the best fit parameters [25] showed that the native defects associated with a Te-rich crystal is believed to be mainly doubly ionized Cd-vacancy acceptor

with essentially no ionized Te anti-site donor [26]. Secondly, if the composition of Te becomes high than 0.50012, i.e. the maximum of homogeneity range, the solidified crystal will consist of a mixture of CdZnTe solid and a Te-rich second phase, which was usually stated as Te inclusion/ precipitate. Even if the shift in Te composition is not larger than 0.50012, with the usually slow cooling rate after the growth, the solidified crystal might still have the Te-rich precipitates embedded inside because of the retrograded nature of the solidus curve. Therefore, it is recommended to provide the equilibrium partial pressures over the melt during crystal growth to maintain the condensed phase as close as possible toward stoichiometric composition. Strictly speaking, one needs to investigate the thermodynamics of the Cd-Zn-Te system to determine the composition and temperature of a ternary Cd, Zn and Te reservoir that can provide exactly the respective partial pressures of Cd, Zn and Te_2 [27]. However, since the partial pressure of Cd is two orders of magnitude higher than the others, it is usually sufficient to provide a constant Cd over pressure using a pure Cd reservoir. The precise Cd reservoir temperature will be determined by the temperature of the $Cd_{0.8}Zn_{0.2}Te$ melt during the crystal growth and the post-growth cooling.

The measured Cd overpressure, over the melts at different temperatures, can be fit with the equation:

$$\log_{10} P_{Cd}(atm) = -10{,}560/T(K) + 7.702 \qquad \text{Eq. (3)}$$

For the melt growths employing different thermal profiles, e.g. for the melt surface at temperature of 1132, 1150 and 1170°C, the Cd overpressure can be derived from Eq. (3) to be, respectively, 1.53, 1.91 and 2.42 atm, which correspond to a pure Cd reservoir of 805, 826 and 850°C, respectively, from Eq. (1).

3.2 Reduction of Interaction between Samples and Fused Silica Ampoules by HF etching

During the processing of electronic/optical compound semiconductors at elevated temperature, the sample has the tendency to interact with the fused silica container and form chemical bonding, the so-called “wetting”, which makes the sample attaching to the ampoule wall. During the cool-down of the sample after the processing, as the bulk of the sample goes through larger thermal contraction than fused silica, the wetting area remains attaching to the fused silica wall and, consequently, causes the sample to separate apart which causes cracks and other structural defects. These defects are detrimental to the electronic/optic performance of materials, especially on the applications of high-quality compound semiconductors.

The severity of the chemical interaction between the sample and fused silica inner-wall depends on several factors: (1) the chemical activity of the sample and the fused silica, (2) the processing temperature, (3) the duration at the temperature and (4) the contact area of the interaction. For example, the heating schedule in the homogenization of HgCdTe was designed to reduce the chemical activity of Cd by annealing it first at lower temperature to eliminate the wetting [28]. A dewetted growth of CdTe was practiced on earth, provided by a gas pressure in the crucible which equalized the hydrostatic pressure in the melt [29]. But the contactless growth was stable only for the first 25 mm of the growth because of the changing of the solid-liquid interface shape. In general, the first three of these factors are case-dependent, i.e., they are different for various material systems as well as different processing conditions. To find a general solution for each different case, it is desired to focus on the fourth factor, i.e., to reduce the contact area between the sample and the container. The total area that the grown crystal contacting the container depends on the surface features of the inner-wall. A very flat and smooth surface provides a large contact area whereas a rough surface, with peaks and valleys, limits the contact area to the peaks due to the surface tension of the melt/crystal. With this

concept, a simple method to modify the surface morphology of the fused silica inner-wall was developed by etching it with HF acid before any crystal growth activity. Typically, the HF rinse of 30 seconds to 2 minutes has been widely adopted in the cleaning of the surface of fused silica inner-tubing before any processing activities. However, a long-time HF etching of 30 minute can modify the surface features of fused silica and affect the interaction between the sample and its container. The effects of the HF etching have been demonstrated [30] in the crystal growth by physical vapor transport of ZnSe and Fe-doped ZnSe as well as melt growth of PbTe compound semiconductors. The method is applicable to all processes involving interaction between materials and fused silica container at elevated temperatures.

3.3 Homogenization of Starting Materials under External Vacuum Environment

The starting materials were prepared from 99.99999% purity Cd and Zn with 99.9999% purity Te. The weighed elements were loaded inside fused silica ampoules, which have been previously cleaned, HF etched and baked out under vacuum. The loaded ampoules were evacuated and sealed under vacuum condition. Because of the large mass of the sample, above 300 g, the ampoules sometimes explored inside the rocking furnace during heating up. It was concluded that the exothermic Te eutectic reaction between metals and Te released a large amount of energy, which rapidly raised the sample temperature and caused the instantaneous jump of vapor pressure inside the ampoule. To mitigate this problem, the loaded homogenization ampoule was first gone through a localized eutectic reaction by a traveling zone process. The procedure was similar to a zone melting process except that the zone temperature was set to be just high enough, about 510^{o}C, to induce localized Te eutectic reaction (about 450^{o}C). The zone traveled at 15 to 20 cm/h and a sponge-like sample was formed after the zone process.

For the first few runs, the homogenization ampoules were loaded inside a resistance heated tubular furnace for the melting and mixing of the charge. The spongy-looking material was heated up to 1070^{o}C, soaked for 36 h, then was raised to 1160 ^{o}C, rocked for 3 to 5 h before casting by turning off the furnace power vertically. However, the electrical properties and the impurity analysis of the grown crystals, as shown in the later section of characterization, implied the contamination of Cu, C and O impurity. During the later runs, the contamination was successfully minimized by loading the homogenization ampoules inside another closed tubing of fused silica with a larger diameter, which was pumped to provide a vacuum of 10^{-3} Torr during the homogenization process. Even with the modified homogenization process and the controlled Cd overpressure, the electrical property of undoped grown crystals was not consistent, with the electrical resistivity, ρ, varied from 10^{3} to 10^{8} Ω-cm. By adding the intentional Indium dopant, 4 to 6 ppm (atomic), to the pure elements during homogenization, the electrical resistivity of the grown samples were consistently above 10^{8} Ω-cm when the Cd reservoir was maintained between 785 and 825^{o}C, with details given in later sections.

3.4 Mechanical Pulsed Disturbance to Promote Single Crystal Growth

For certain semiconductors with important applications, the existing unseeded bulk growth of directional solidification from the melt usually results in poor-quality multi-crystalline ingots which cause the low yield of the commercial growth process. The multi-grained crystal growth was partially caused by the large supercool of the melt, which not only results in a large section of ingot solidifying uncontrollably under spontaneous nucleation [31] but also prohibits the ideal growth condition that single crystal nuclei forming at the very tip of the ampoule and growing into large single grains. The DTA measurements on a CdTe sample [32] started with heating the sample up rapidly to above its melting point of 1092 ^{o}C and, after soaking for 9 h, a

furnace cooling rate of about 10°C/min commenced. During the cooling of the furnace, the sample temperature stayed at 1092°C and eventually started to decrease when the furnace reached 1040°C, i.e., a supercooling of 50°C. The degree of supercooling was also reported [33] to be correlated to the Cd partial pressure over the CdTe melt where the supercooling was studied by measuring the electrical conductivity during solid-liquid transition. It was found that the degree of superdooling decreases from 23°C, 13°C, to 8°C when the Cd overpressure was raised from 1.3 atm, 1.4 atm, to 1.6 atm, respectively.

To prevent the undesired formation of a large multi-grained spontaneous nucleation, i.e., to promote nucleation under the condition of small supercooling, a short-time mechanical perturbation was applied to the growth ampoule at a critical time during growth when the melt at the ampoule tip just reached below the liquidus temperature. The technique was implemented to the directional solidification process of $Cd_{0.80}Zn_{0.20}Te$ crystals [32] by adding a solenoid AC vibrator, which was bound to the extension of the growth ampoule, with a frequency of 60 Hz and an adjustable magnitude. The high-frequency shaking of the ampoule for 10 to 30 sec causes local inhomogeneity in the supercooled melt, which promotes the nucleation in the melt and, consequently, a small section of solid, usually single or double grain, was formed at the growth tip which grew continuously throughout most of the ingot length.

3.5 Crystal Growth and Post-growth Cooling

The growth ampoule was made of fused silica with diameter ID x OD from 20mm x 25mm to 40mm x 45mm and a tapered length of 2.5 cm at the growth tip. The ampoules were cleaned, HF etched and baked at 1180 °C under vacuum condition for 16 h. The homogenization ampoules were opened and the starting materials were ground into particles with dimension less than 5 mm. After the starting material has been loaded inside the growth ampoule, a basket

holding about 2 g of pure Cd was inserted on the top of the ampoule as the Cd reservoir, which was fixed beneath the seal-off cup. The ampoules were then sealed under a vacuum lower than 10^{-5} Torr.

The Bridgman growth furnace was set up vertically with four independently controlled electrical-resistance heating zones. A typical thermal profile and the initial ampoule position are shown schematically in Figure 4. The thermal profile was provided by the heating zones of, from top to bottom, the Cd reservoir zone (which was equipped with a heat pipe – the isothermal furnace liner), the hot zone, the booster zone and the cold zone. The liquidus temperature of $Cd_{0.8}Zn_{0.2}Te$ was determined to be between 1115 and 1132°C [19,34,35]. Figure 4 shows that the starting melt was about 7 cm long and a total length of 32 cm is required for the growth ampoule so as to maintain the starting melt above 1130°C with a positive thermal gradient (to prevent bubbling in the melt) and an independently controlled Cd reservoir on the top of the ampoule. The melt was soaking for at least 48 h at 1145°C in order to completely dissolve any local clusters of Te-rich chains as reported in Ref.[36-38] that clusters, in the forms of branched chains of Cd_nTe_{3n+1} or Te atoms, was observed in $Cd_{1-x}Zn_xTe$ ($0 \leq x \leq 0.1$) during the dynamic viscosity measurements. The Cd reservoir temperature from 750 to 935°C was employed with the range of 785 to 820°C used for most of the runs. The furnace translation rates were 0.75 to 2 mm/h (mostly used).

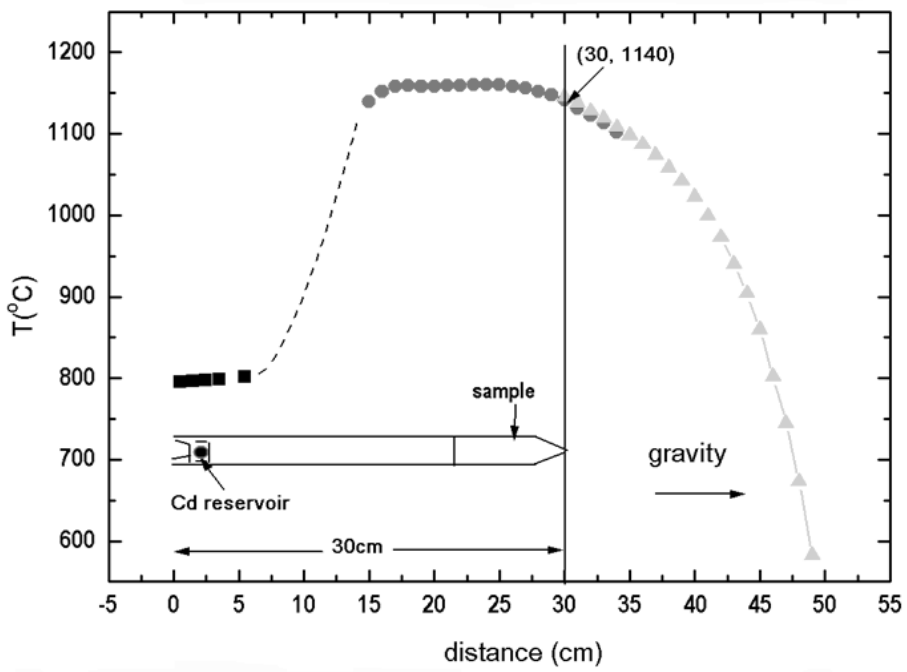

Figure 4. The thermal profile and the initial ampoule position for a typical crystal growth.

After a furnace translation time of 100 to 125 h, the solidified sample and the Cd reservoir were cooled down to room temperature with constant rates over a period of 96 to 144 hours. However, after slicing the ingots perpendicularly, the measured electrical resistivity of the sliced disc was not uniform across the radial section [39]. For instance, on the wafer cut at 2.5 cm from the tip of ingot CZT-26, with a Cd reservoir of 785°C, the center of the ingot showed electrical resistivity of 2 x 10^9 Ωcm, whereas the resistivity at the edge was 40 Ωcm. An adjustment of cooling schedule was adopted for the CZT-29 run. The environments of the CZT-26 and -29 ingots at the end of crystal growth and during the 2 days' cooling are shown in Figure 5 as red and black boules, respectively, relative to the three-phase diagram of Cd given in Figure 2(b). As shown in the top-left corner of the figure, at the end of growth, when the top of the

ingots was at the solidus temperature, 1115 ºC, the tip of the 8 cm long crystals was at 995 ºC, as deduced from the thermal profile of the growth furnace. During the late-stage of growth and long duration of cooling, the Cd overpressure of CZT-26 was too high, especially for the earlier grown section, which caused the Cd atoms to diffuse into the ingot surface and shifted the stoichiometry of the surface region. To optimize the environment of Cd overpressure, the Cd reservoir temperature was programmed to cool down for 50 – 80ºC in the last 55 – 75 h of furnace translation. Figure 5 shows that, for the growth of CZT-29, the Cd reservoir temperature cooled down from 785 to 735ºC in the last 70 h of growth. So at the end of the furnace translation, while the whole CZT-26 sample was in equilibrium with a Cd pressure of 1.7 atm the Cd overpressure over CZT-29 was 0.69 atm. The electrical properties measurements confirmed the radial uniformity of the CZT-29 crystal. The black solid line in Figure 5 for CZT-29 corresponds to the optimal temperatures for the crystals and the Cd reservoir during the post-growth cooling. In an effort to grow inclusion-free single crystal of CdTe, Franc et al. [20] have reported the stoichiometric line of Cd overpressure, defined by $x_{Cd} = x_{Te} = 0.5$, during the growth of CdTe as P^S (atm) = $8 \times 10^5 \exp(-1.76 \times 10^4/T)$. A comparison between their P^S and our optimal P_{Cd} for CZT-29 shows that the two lines are in the same pressure range with the slope of their line a bit steeper than ours. For instance, at the temperatures of 995, 743, and 510ºC, respectively, the values for P^S are 0.75, 0.024, and1.4×10^{-4} atm and our optimal pressures are 0.46, 0.032, and 5.2×10^{-4} atm. However, the differences between these two lines should be pointed out. Firstly, the P_{Cd} line for CZT-29 is the optimal line to maintain a constant stoichiometry of the grown crystal during the cooling process, whereas the P^S from Ref. [20] was the stoichiometric line for $x_{Cd} = x_{Te} = 0.5$. Secondly, the compositions of the crystals are different, i.e., $Cd_{0.8}Zn_{0.2}Te$ in our case and CdTe in their study.

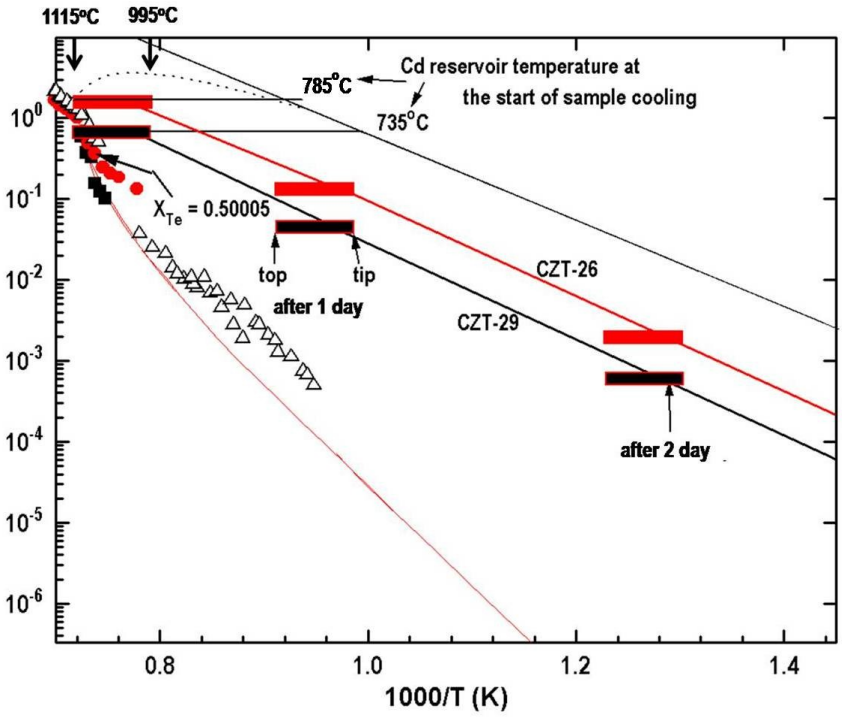

Figure 5. The Cd three-phase loop for $Cd_{0.80}Zn_{0.20}Te$ and the stoichiometric positions for CZT-26 and CZT-29 during post-growth cooling (taken from Figure 3 in Ref.[39]).

4 Characterizations

The crystalline quality and morphology of the grown crystal was first examined by visual observation on the as-grown ampoule. Then the cylindrical crystal was sliced perpendicularly by a wire saw at specific locations from the first freeze tip and a 2 mm thick wafer was obtained. A 2x2x20 mm prism was sliced from the wafer for the chemical analysis of Glow Discharge Mass Spectroscopy (GDMS) provided by Shiva Technologies. Other samples were sliced, lapped and mechanical polished for the subsequent Hall measurements. Slices from crystals grown under different Cd reservoir temperatures were prepared by lapping and polishing for the examinations under IR microscope to study the structure defects, especially for the size and density of Te inclusions.

4.1 Crystalline Quality and Morphology by Visual Observations

4.1.1 Effects of the HF etching pre-treatment. The effects of HF etching on the reduction of interaction between samples and fused silica ampoules were visually examined on the as-grown ampoules and the results are shown in the pictures below. Figure 6(a) shows the grown crystal without the pre-treatment of HF etching. Although the grown ingot was single crystal, it broke into three long axial pieces as shown in the inset at lower-left corner. Presumably, at least three wetting areas caused the sample surface to attach to the inner wall of the ampoule and separate the ingot axially into three pieces during cooling. Usually, the HF-treated samples detached from the wall intact and slid freely inside the ampoules by applying gentle horizontal movements as shown in Figure 6(b).

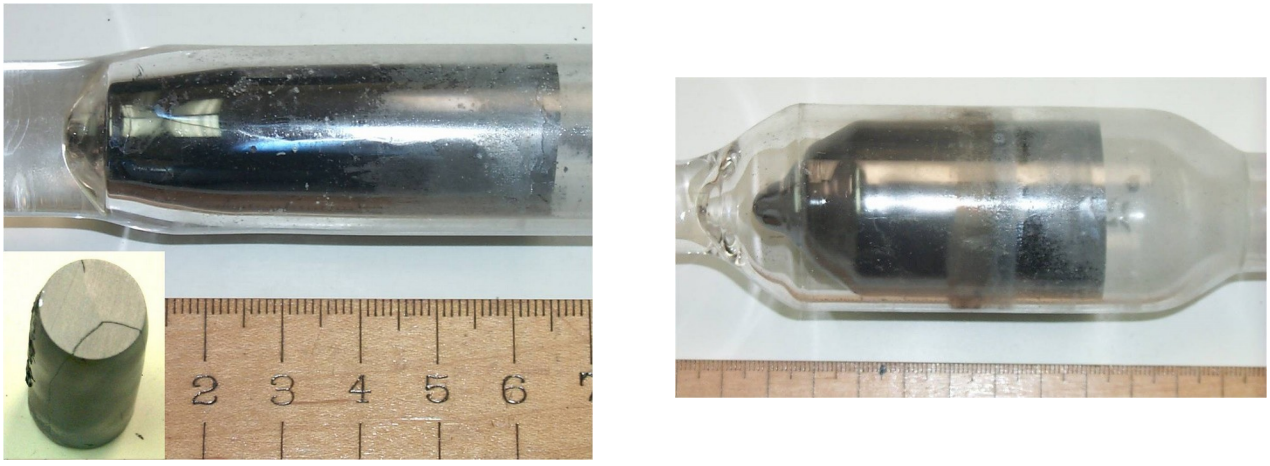

(a) **(b)**

Figure 6. The pictures of two as-grown CdZnTe ampoules. (a) CZT-39 ampoule: without HF-treatment resulted in the sample separating axially into three pieces as shown by the inset (b) CZT-36 ampoule: with HF-treatment, as-grown sample detached and slid inside the ampoule.

4.1.2 Effects of Mechanical Disturbance. The growth environments and procedures for two 20 mm diameter ingots of CZT-37 and CZT-38 were implemented as similar as possible

except that the mechanical tapping was introduced to the latter but not the former. They were both grown with furnace translation of 1.25 mm/h, growth time of 125 h and cooling time of 96 h except the values for (total mass, Cd reservoir temperature) was (95.2 g, 820^{o}C) and (91.9g, 805^{o}C) for CZT-37 and -38, respectively. Figure 7(a) shows that the cross section of CZT-37 at 1.5 cm from the tip has at least five grains and some twinnings and the cross sections at 1.8 cm and 2.5 cm, given in Figure 7(b), also exhibit multiple grains. Figure 7(c) shows that the slices cut at 1.5 cm and 1.8 cm from the ingot CZT-38 which exhibit a mono-crystalline structure. The cross section at 1.5 cm has some twinnings which disappeared at the cross section of 1.8 cm. The longitudinal cut of the remaining CZT-28 ingot shown in Figure 7(d) extends the mono-crystalline structure through the ingot till the last 1.0 cm section which resulted in coverage of single grain more than 70% of the ingot. The single crystallinity has been confirmed from the X-ray diffraction spectra.

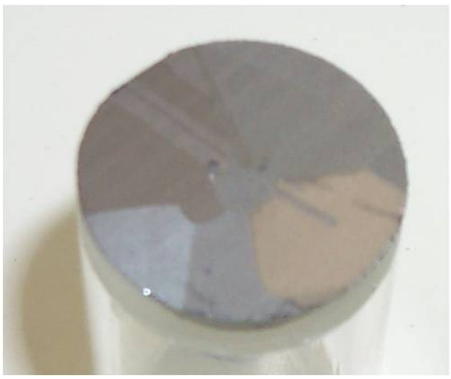

(a)

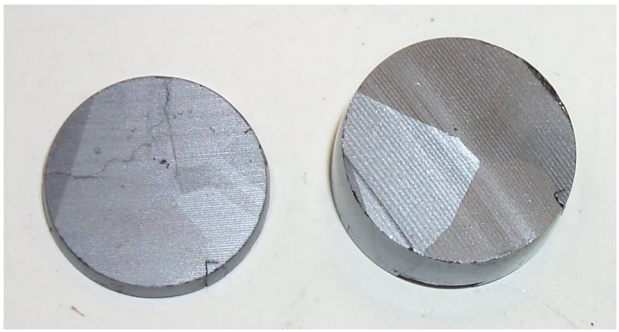

(b)

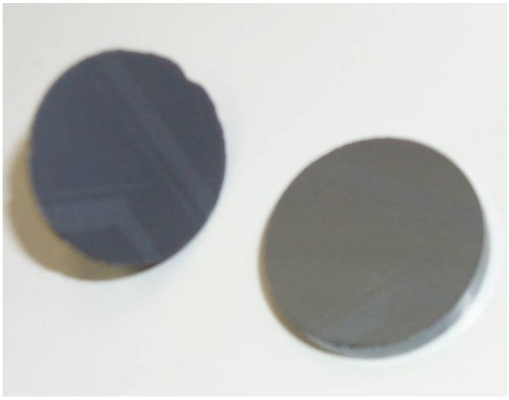

(c)

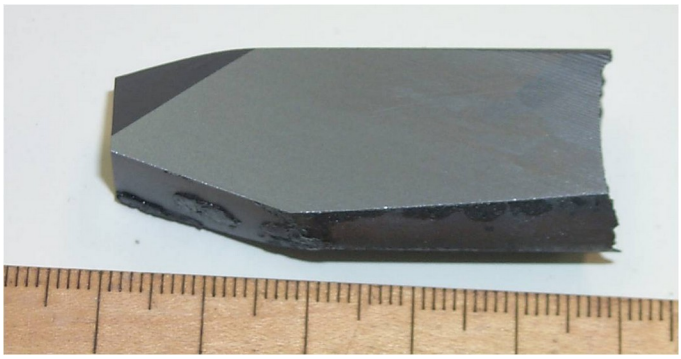

(d)

Figure 7. CZT-37, grown without the mechanical perturbation: (a) shows the cross section at 1.5 cm from the tip and (b) show cross sections at 1.8 cm and 2.5 cm. CZT-38, grown under the same conditions as CZT-37 except that the mechanical perturbation was applied: (c) shows the slices cut at 1.5 cm and 1.8 cm from the ingot and (d) shows the longitudinal cut of the remaining ingot.

Several 40 mm diameter ingots have also been processed with and without mechanical disturbance. Without the mechanical perturbation, as shown in Figure 8(a), the as-grown ingot of CZT-16 shows multiple crystalline grains with twins. Another grown ingot without mechanical tapping, CZT-20, as shown in Figure 8(b), also exhibits multiple grains. On the other hand, the ingot of CZT-36, grown with the mechanical perturbation, which slid inside the growth ampoule as shown in Figure 6(b), was sliced axially from the tip to 2.5 cm. The first-grown section shows two grains in the tapered shoulder area as given in Figure 8(c). Twinnings occurred in one of the

grain but they were limited to the first 1.5 cm section. The ingot developed into one major and one minor crystalline grain, as shown in the cross section area at 2.5 cm given in Figure 8(d), with the major grain covering more than 70% of the sample.

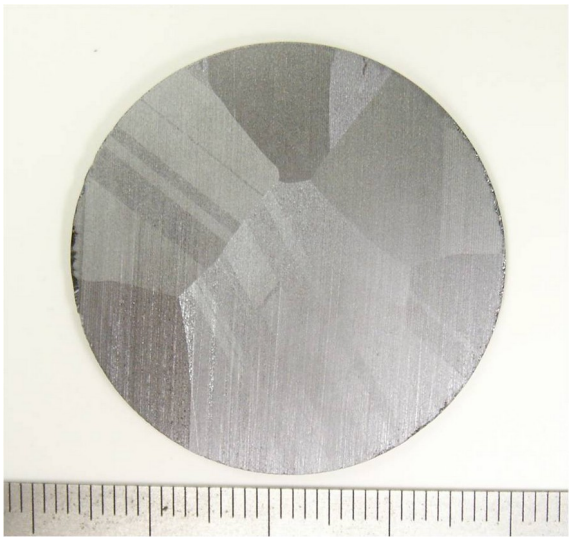

(a)

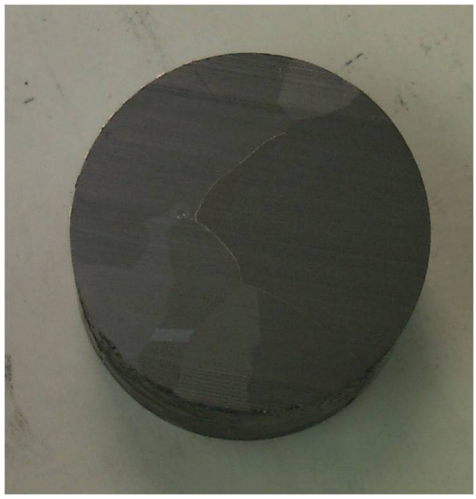

(b)

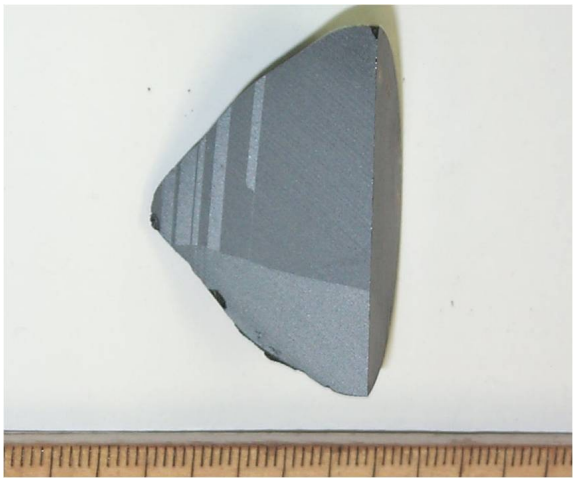

(c)

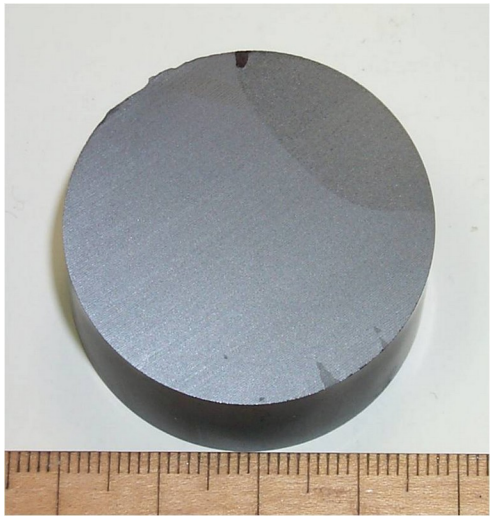

(d)

Figure 8. Two 40 mm diameter ingots grown without the mechanical perturbation: (a) multiple crystalline grains with twins in the grown ingot of CZT-16 and (b) multiple grains in the grown ingot of CZT-20. The 40 mm diameter ingot, CZT-36, grown with the mechanical perturbation: (c) the axially sliced section of the first 2.5 cm sample showing two grains with twins in the tapered shoulder area and (d) the cross section area at 2.5 cm from the grown tip with the major grain covers more than 70% of the sample.

4.2 Chemical Analysis

The effect of homogenization under external vacuum condition was evaluated by chemical analysis. The impurity concentrations of samples cut from the crystals were analyzed by GDMS and the results from two undoped ingots are described here. The growth conditions for the two runs were similar: the furnace translation rate was 1 mm/h for both runs and the Cd reservoir temperatures were 770 and 805 ^{o}C for CZT-2 and CZT-9, respectively. The major difference was that CZT-2 was homogenized in an atmospheric environment, whereas CZT-9 was homogenized in an external pressure of less than10^{-3} Torr vacuum condition. Table 2 presents the analyses of two samples cut at 2.5 cm from their first-to-freeze tips. The results show that homogenization in the vacuum environment significantly reduces the impurity concentrations in the grown crystals, especially in the concentrations of the major impurities Cu, C, O, and Fe. The electrical conductivity measurements were performed on the remains of these two wafers. The results were consistent with the GDMS analysis that the measured p-type electrical resistivity of $8x10^{4}$ Ω-cm and $3x10^{9}$ Ω-cm, respectively, for the CZT-2 and CZT-9 2.5cm samples.

Table 2. The impurity concentrations (in ppb, atomic) measured by GDMS on samples cut from the grown crystals of CZT-2 and 9.

Sample	CZT-2; 2.5cm	CZT-9; 2.5cm
Element	Concentration	Concentration
C	980	20
N	45	15
O	980	35
Na	12	54
Mg	170	27
Al	26	7
Si	11	8
S	230	280
Cl	56	49
Cr	28	67
Mn	< 10	60
Fe	480	93
Ni	23	46
Cu	3300	110
Se	160	210

4.3 Electrical properties measurements

A Lake Shore, Model 7500 Hall Effect Measurement Systems with a magnetic field strength up to10 kG was used for the measurements of the electrical properties. The cut wafers were chemical-mechanical polished to about 1 mm in thickness and electrical contacts were made by depositing Au film, using RF sputtering. The Hall data measurements confirmed that the contacts were ohmic. The measured resistivities of the In-doped samples grown with Cd reservoir between 785 and 825^{o}C were consistently higher than 10^{8} Ω-cm and up to $2x10^{11}$ Ω-cm. Two quantities, electrical resistivity and Hall coefficient, were measured which

are determined by four material parameters, namely, electron concentration, n, hole concentration, p, electron mobility, μ_n, and hole mobility, μ_p. The governing equation for resistivity, ρ, is given by

$$\rho = 1/(ne\mu_n + pe\mu_p) \quad , \tag{3}$$

and the equation for Hall coefficient, R_H, under the condition $\mu_n >> \mu_p$ (as is the case in CdZnTe) can be expressed as:

$$n = \frac{1}{\rho e \mu_n}\left(\frac{\mu_p}{\mu_n} - \frac{R_H}{\rho \mu_n}\right) \quad . \tag{4}$$

To obtain the electron and hole concentrations, the values of 1000 and 100 cm^2/Vs for the electron and hole mobilities, respectively, measured on $Cd_{0.8}Zn_{0.2}Te$ samples at room temperature [40], were used. Table 3 lists the measured Hall coefficients and resistivities at room temperature, and the calculated electron and hole concentrations for two ingots, CZT-26 and CZT-29; both were doped with In (4.2 ppm, atomic) and grown with a Cd reservoir at 785 °C. Since the CZT-26 wafer showed radial nonuniformity in electrical properties, the values given here are for the center section of a wafer cut at 2.5 cm from its tip. The CZT-29a and -29b samples were sliced at 2.5 and 4.0 cm, respectively, from the tip of CZT-29.

Table 3. The measured Hall coefficients and resistivity, ρ, at room temperature, and the derived electron and hole concentrations, n and p, from two grown ingots, CZT-26 and CZT-29 (taken from Table 1 of Ref.[39]).

Sample	Hall coeff. [cm^3/C]	ρ [Ω cm]	n [cm^{-3}]	p [cm^{-3}]
CZT-26; 2.5 cm	8.9×10^{9}	2.1×10^{9}	3×10^{5}	2.8×10^{6}
CZT-29a; 2.5 cm	-1.84×10^{13}	8.4×10^{9}	$\sim1.7\times10^{6}$	$<10^{6}$
CZT-29b; 4.0 cm	-1.2×10^{11}	1.2×10^{9}	1×10^{6}	4×10^{7}

4.4 Infrared (IR) Transmission Microscopy

The IR transmission images were taken on sliced and polished wafers, about 2 mm thick, by an IR camera and IR microscope to study the structural defects, such as cracks, grain boundary, twins as well as Te precipitates. The IR transmission image of a typical 20 mm diameter single crystal wafer, presented in Figure 9(a), shows no evidence of grain boundary and twin. Some foggy line segments might have been the images of polishing lines on the surfaces. Figure 9(b) shows the image from IR microscope taken on a wafer sliced from a crystal grown under a Cd reservoir of 717 ^{o}C. With the scale of 1 mm, the size of the small dots, presumably Te precipitates, range from 10 to 20 μm. The identity of the three larger particles, with the size of the lower-right corner at 65 μm, is not clear. They might have been the Te inclusions from the engulfment of Te-rich liquid droplet due to the fluctuation of the growth interface. Figure 9(c) – 9(f) show the IR micrographs from crystals grown under Cd overpressure with increasing Cd reservoir temperature (given at the bottom of each image). From the trend of the Te precipitates density, it was concluded that a Cd reservoir temperature of 820$\pm$10 ^{o}C resulted in the lowest precipitate density which agrees with the required equilibrium P_{Cd} of the Cd reservoir at 820 ^{o}C over the $Cd_{0.8}Zn_{0.2}Te$ melt at 1145^{o}C, shown in Figure 2. As a comparison, inclusion-free CdTe crystal was grown by vertical Bridgman technique using a Cd overpressure of 850°C with a melt temperature of 1118°C [41].

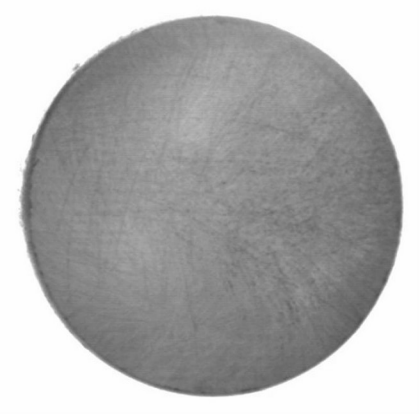

(a) CZT-34

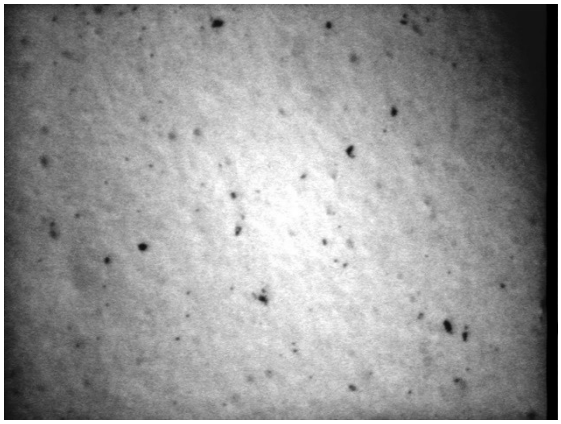

(d) 800 ºC

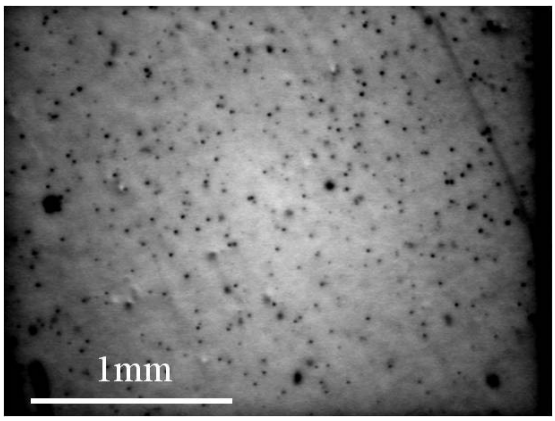

(b) 717 ºC

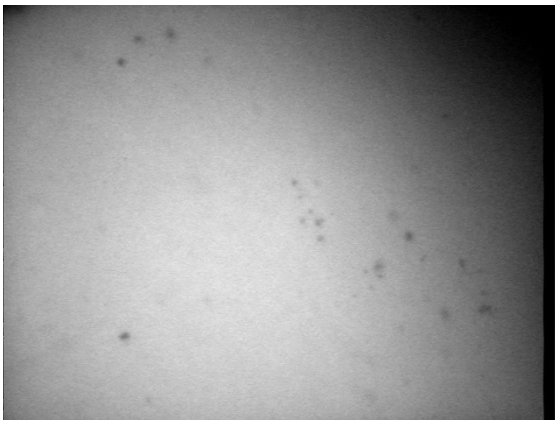

(e) 825 ºC

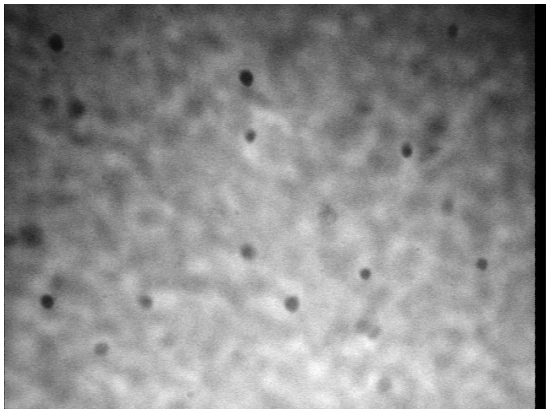

(c) 747ºC

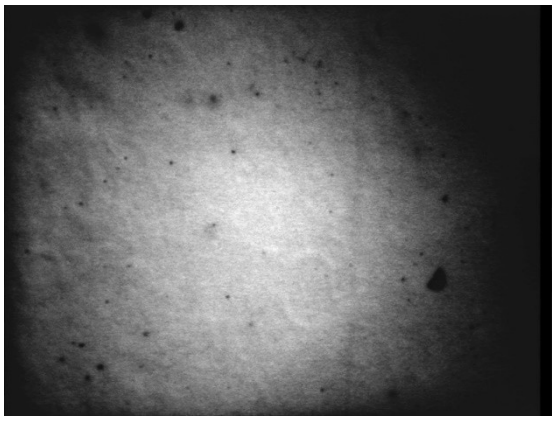

(f) 843ºC

Figure 9. (a) An IR transmission image of a typical 20 mm diameter single crystal wafer; (b) – (f) transmission images of IR microscope taken from wafers sliced from crystals processed under different Cd reservoir temperatures.

4.5. Thermoelectric Properties of CdZnTe

The thermal conductivity is one of the thermophysical properties needed for any meaningful simulation of the growth process. The extreme high level of electrical resistivity at room and cryogrnic temperatures makes it difficult to interpret the results. The measurements of a lower electrical resistivity in the elevated temperature together with Seebeck coefficients can provide an in-depth understanding of the electrical conduction mechanisms in the crystals. Therefore, the thermal conductivity, electrical conductivity, and Seebeck coefficient of a vapor-grown CdTe and two melt-grown $Cd_{0.8}Zn_{0.2}Te$ crystals, including In-doped CZT-30 and un-doped CZT-34 samples, were measured between 190ºC and 780ºC to study the thermoelectric properties of CdZnTe. Additionaly, from the three sets of measurements it would be interesting to investigate the thermoelectric properties of CdZnTe since there have been very few evaluations [42] on the potential thermoelectric applications of this wide band gap semiconductor system.

4.5.1 Crystal Growth by physical vapor transport (PVT). The CdTe crystals have been grown by a horizontal seeded PVT process [43,44]. The present measurements were performed on the crystal of CdTe-15 which was grown with the following procedures. After a CdTe single crystal seed with growing face of (112) was positioned in a fused silica growth ampoule of 16 mm ID, 22.7 g of homogenized CdTe (x_{Te} = 0.50002) starting material was loaded. The loaded ampoule was baked under vacuum at 880ºC for 5 minutes to adjust the stoichiometry of the starting material before sealing off under vacuum. During the growth, the CdTe source was maintained at 880ºC with a temperature bump and gradient of 35ºC/cm at the super-saturation location where the seed surface was positioned. After 281.5 h of growth with furnace translation

rate of 0.158 mm/h, the furnace was cooled to room temperature in 32 h. All of the starting material has been transported.

4.5.2 Thermoelectric property measurements. The single crystal samples, in the shape of 20 mm diameter and 3.0±0.5 mm thick disc, were cut perpendicularly to the growth axis from the grown crystals by a wire saw. The slices were 2.4 cm, 2.6 cm, and 2.4 cm from the first grown location for CdTe-15, CZT-30, and CZT-34, respectively, and were characterized by the following.

4.5.2.1 Thermal conductivity. The thermal conductivity, κ, was determined from the following equation:

$$\kappa = \rho C_p \alpha \qquad \text{Eq. (4)}$$

where ρ, C_p, and α are density, heat capacity, and thermal diffusivity, respectively. The thermal diffusivity was measured by the Flashline 3050 System from Anter Corp. (now TA Instruments) between room temperature and 760°C. In the flash technique, when the sample was heated and in equilibrium with a preset temperature, the radiant energy of a high-intensity light pulse was absorbed on the front surface of the disc and the resultant temperature rise on the rear face was recorded. The diffusivity was calculated from the thermogram using the Clark and Taylor analysis [45]. For each temperature, the diffusivity was taken from the average of three successful measurements.

The density of CdZnTe was calculated from the lattice constants, *a*, of CdTe and ZnTe from the Vegard's law:

$$a(Cd_{1-x}Zn_xTe) = (1-x)\, a(CdTe) + x\, a(ZnTe) \qquad \text{Eq. (5)}$$

The room temperature lattice constants have been reviewed by Williams [46] to be 0.6481 and 0.6103 nm, respectively, for CdTe and ZnTe. The density at elevated temperature was determined by the lattice constant values at room temperature and their linear thermal expansion coefficients values reviewed in Ref. [46] and in Ref. [47] for CdTe and ZnTe, respectively.

As described earlier, the partial pressure of Zn can be derived from the results of the best fit quasi-regular interaction parameters determined in Ref. [19] for the CdTe-ZnTe solid solution. In a quasi-regular solution of $Cd_{1-x}Zn_xTe$, the heat capacity, C_p, is given by:

$$C_p(Cd_{1-x}Zn_xTe) = (1-x)\, C_{p(}CdTe) + x\, C_p(ZnTe) \qquad \text{Eq. (6)}$$

where the heat capacity for CdTe was adopted from K.C. Mills [48] to be

$0.1668 + 1.377 \times 10^{-4}$ T(K) (J/g-K) and C_p(ZnTe) is given by $0.2407 + 5.638 \times 10^{-5}$T(K) (J/g- K) [49].

4.5.2.2 The electrical conductivity and Seebeck coefficient. The electrical conductivity and Seebeck coefficient were measured simultaneously by the ULVAC ZEM-3 instrument from room temperature to 800°C. The samples were sliced into the shape of roughly 2x2x15mm rectangular prism. The electrical conductivity was determined from ten measured I-V points and the Seebeck coefficient was derived from the values of Seebeck voltages measured over 6 mm distance along the sample under three different applied thermal gradients.

4.5.3 Results and analysis.

4.5.3.1 Thermal conductivity. The measured thermal conductivities from room temperature to 750°C for the three samples are given in Figure 10. The thermal conductivity of CdTe was slightly above 0.08 W/cm-K at room temperature, decreased to and stayed around 0.035 W/cm-K when temperature reached above 200°C, then slowly decreased when temperature

reached above 700°C. The thermal diffusivity of CdTe has been measured by a similar laser-flash method between 930 and 1085°C [50]. Their thermal diffusivity data were multiplied by the values of heat capacity and density at the temperatures to obtain the values for thermal conductivity which are also shown in Figure 10. Those data are in line with the extension of present data from the lower temperature range.

The thermal conductivity for the In-doped CdZnTe, CZT-30, stayed below 0.03 W/cm-K in the low temperature range with a shallow minimum at about 250°C. The un-doped CdZnTe sample, CZT-34, has the thermal conductivity similar to that of CZT-30 in the low temperature range and increased to a slight maximum at about 650°C. All three sets of the thermal conductivity data merged together at about 750°C – an implication that the samples became intrinsic as the phonon contribution to thermal conductivity started to dominate at elevated temperatures.

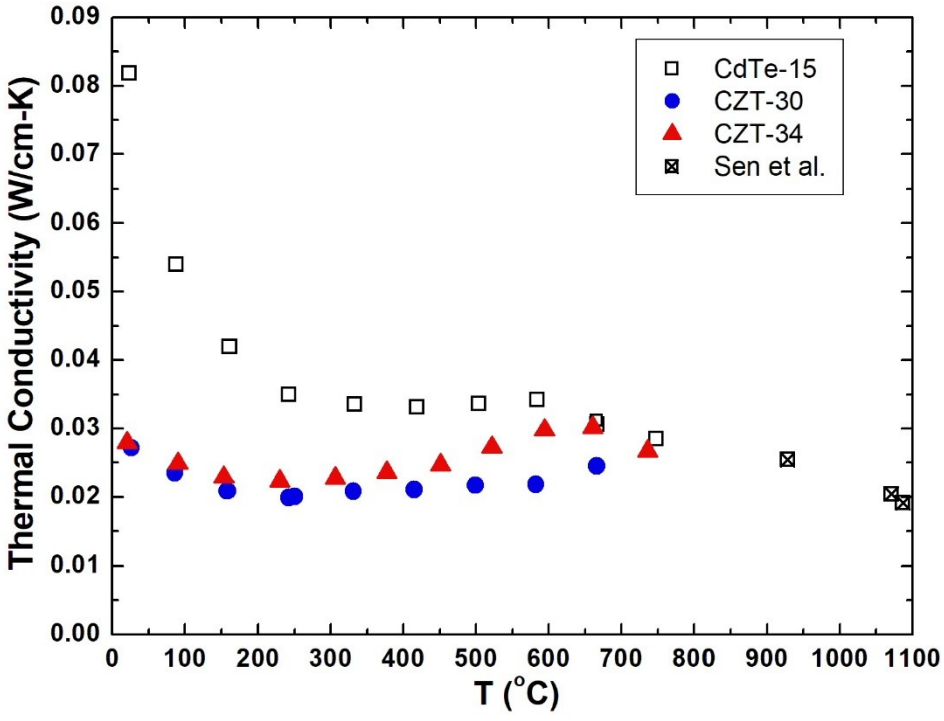

Figure 10. The measured thermal conductivity for CdTe, In-doped (CZT-30) and un-doped (CZT-34) $Cd_{0.80}Zn_{0.20}Te$ samples plotted against temperature. The three data for CdTe

(Sen et al.) at temperature above 900°C are from Ref. [50] (taken from Figure 1 of Ref. [42])

4.5.3.2 Electrical conductivity. The measured electrical conductivities for the three samples are plotted in log scale vs. 1000/T(K) as shown in Figure 11. The CdTe crystal, grown from a starting material being heat-treated to approach congruent sublimation condition [44], contains very small amount of native defects (donor or acceptor) and hence is close to be intrinsic as evidenced from the almost linear dependence of its electrical conductivity (in log scale) vs. 1000/T, especially for temperature above 440 °C, or 1000/T < 1.4. High temperature electrical conductivity of CdTe single crystals have also been measured previously in the temperature range from 400 to 1200°C [51], shown as a line segment in the figure, are about 50% higher than the present data.

The data for the In-doped CdZnTe, CZT-30, showed low values of electrical conductivity in the low temperature range and also show the intrinsic characteristics by forming a linear line roughly parallel but lower than those data for CdTe due to the larger band gap of CdZnTe. It has been shown that the intrinsic carrier concentration of CdTe can be fitted well [52] by the following form for a non-degenerate semiconductor with parabolic valence and conduction bands:

$$n_i = NT^{3/2}\exp(-E_g/2kT) \qquad \text{Eq. (7)}$$

where N is a constant (related to band structure parameters), T in K, E_g the effective band gap energy, and k the Boltzmann constant. From the measurements of optical transmission at 300 K on CdZnTe [53], the measured cut-on energy for x = 0 and 0.20 was 1.464 and 1.572 eV, respectively. Assuming the band gap difference, 0.108 eV, remains the same and similar band

structure parameters at elevated temperatures, the ratio of intrinsic carrier concentration of $Cd_{0.8}Zn_{0.2}Te$ to that of CdTe would be:

$$n_i(Cd_{0.8}Zn_{0.2}Te)/n_i(CdTe) = \exp(-0.108eV/2kT) \qquad \text{Eq. (8)}$$

Assuming that the mobilities for the carriers are the same for $Cd_{0.8}Zn_{0.2}Te$ and CdTe at a fixed temperature, this ratio in eq. (8) will also be the ratio for their individual electrical conductivity. At the temperature of 1000 K, this ratio of n_i would be 0.534 from eq. (8) which is comparable to the ratio of the measured electrical conductivity at 1000 K, as interpolating from Figure 11 to be 0.54. The electrical conductivity of the un-doped CZT-34 sample started with a value of 0.3 S/cm at around 300ºC and decreased to a minimum of about 0.1 S/cm and then merged with the In-doped sample at temperature above 650ºC.

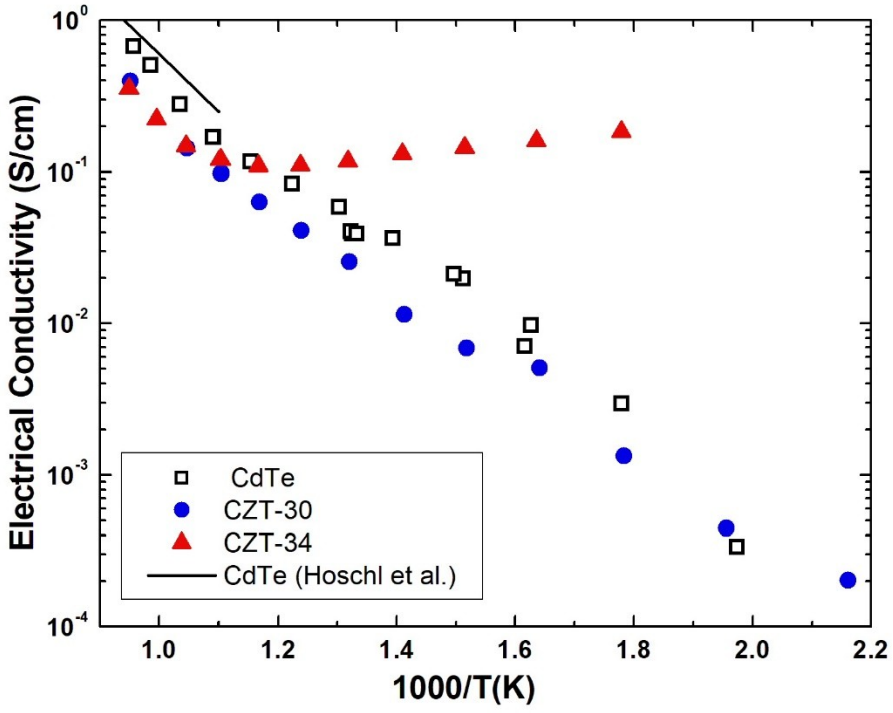

Figure 11. The measured electrical conductivities plotted in a scale of $\log_{10}$ vs. 1000/T(K). The line segment at the upper left corner shows data from Ref. [51] (taken from Figure 3 of Ref.[42])

4.5.3.3 Seebeck coefficient. The types of electrical conduction of CdTe-15 were revealed from the Seebeck coefficient measurements as shown in Figure 12. In the low temperature range, the Seebeck coefficients were positive – indicating a p-type dominant conduction, presumably from native acceptors of Cd vacancy. The measured Seebeck coefficients showed a rather high value of 1.1 mV/K at the lowest measured temperature of 346^{o}C. As temperature increased, the measured Seebeck coefficients decreased slowly as sample approached to be intrinsic and the conduction type converted to n-type around 680^{o}C due to the mobility difference – about 300 cm^2/Vs for electrons and 15 cm^2/Vs for holes at 680^{o}C as reported by Smith [54].

The Seebeck coefficients of CZT-30 indicated n-type conduction at low temperature, converted to p-type at about 250^{o}C, reached a maximum of 0.9 mV/K between 400 and 500^{o}C, and converted back to n-type at 770^{o}C. The small amount of n-type In doping compensated the residual native acceptor Cd/Zn vacancy and showed n-type characteristics in the low temperature range. As temperature increased, the ionization of native acceptors converted the sample into the p-type conduction until at even higher temperatures when the sample approached to be intrinsic and the conduction type converted to back n-type due to the high mobility of electrons.

The Seebeck coefficients measured on un-doped CZT-34 sample in Figure 12 showed p-type conduction at low temperatures with a plateau of 0.97 mV/K between 250 and 550^{o}C then merged with In-doped CZT-30 and converted to n-type at 770^{o}C. The trend confirms that, for the un-doped sample, the native acceptor was formed from the Te-rich range of stoichiometry during the solidification. The Figure of Merit for thermoelectric application, zT, defined as

$$zT = \alpha^2 \sigma T/\kappa \qquad \text{Eq, (9)}$$

where α is the Seebeck coefficient, σ the electrical conductivity, T the temperature in K, and κ the thermal conductivity. The calculated values of *zT*, as hown in Figure 13, for the three samples between 190 and 780 °C were orders of magnitude lower than the state-of-the-art p-type thermoelectric materials mainly dut to the low values of electrical conductivity. As a simple estimate, the value of *zT* for CdTe can be improved to 1.0 at 500°C if the carrier concentration at 500°C reaches p-type $1x10^{18}$ cm^{-3}, either from native acceptors or intentional dopants. For an estimate on the n-type thermoelectric properties for CdTe at elevated temperature, the large uncertainty in extrapolating the Seebeck coefficient gives a value of *zT* to be 1.2±0.4 for n-type CdTe at 1050°C, comparing to the state-of-the-art value of around 1.0 for the n-type SiGe alloy.

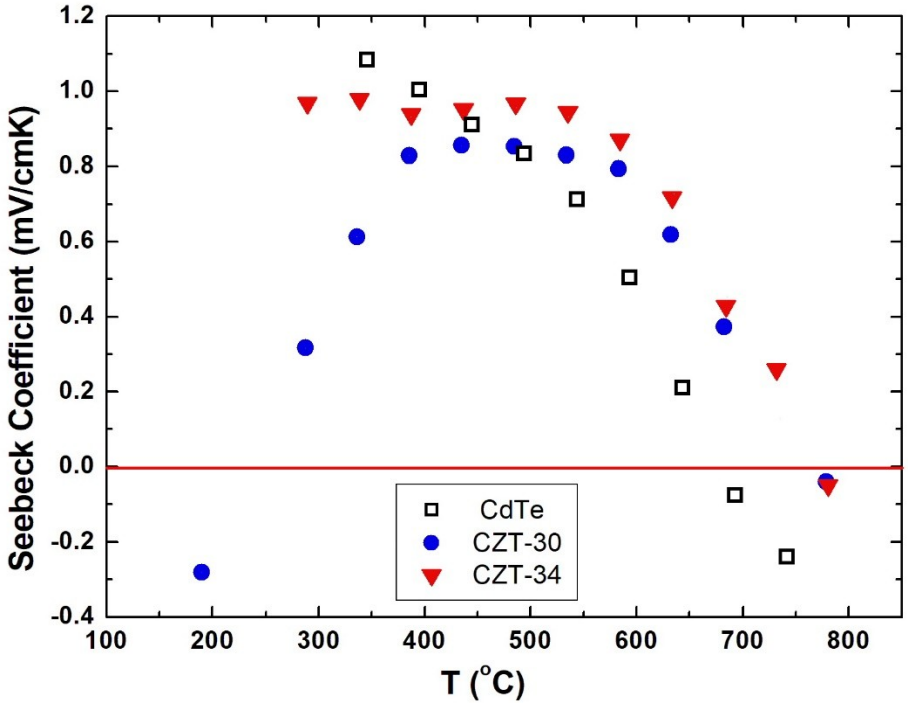

Figure 12. The measured Seebeck coefficient of CdTe, In-doped (CZT-30) and un-doped (CZT-34) $Cd_{0.80}Zn_{0.20}Te$ samples plotted against temperature. Positive and negative Seebeck coefficients represent, respectively, p-type and n-type dominant electrical conduction. (taken from Figure 4 of Ref.[42])

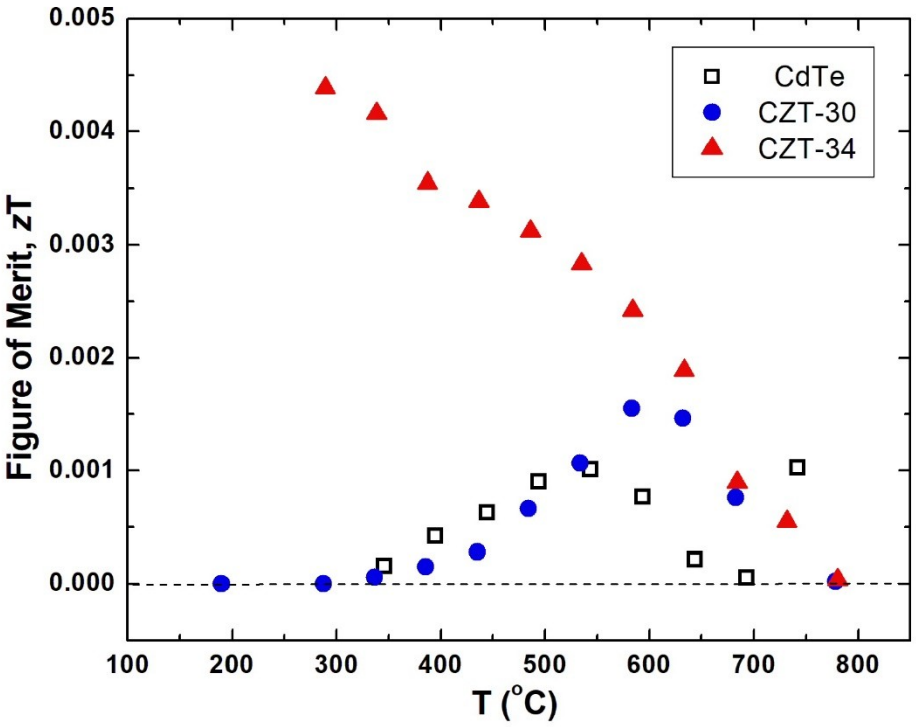

Figure 13. The calculated Figure of Merit for thermoelectric application, *zT*. All of the data are p-type conduction except the data at the two highest temperatures for CdTe as well as the data at the highest temperature for both CZT samples and the lowest temperature for CZT-30 are n-type, (taken from Figure 5 of Ref.[42]).

5 Summary

The data on the composition – temperature – partial pressures (x_{Te}–T – P_{Te2}), corresponding to the Te-saturated $Cd_{0.80}Zn_{0.20}Te$ solid, have been established by measuring the partial pressure using the optical absorption technique. The solidus curve on the Te-rich side of the homogeneity range gives the maximum limit to be $x_{Te} = 0.50012$ at 977 °C. During crystal growth, the measured P_{Cd} in equilibrium with a $Cd_{0.80}Zn_{0.20}Te$ melt, at a temperature of 1145±5°C, is 1.8 atm, which can be provided by a pure Cd reserved of 820°C.

Several procedures have been developed to improve the crystalline quality: (1) a homogenization procedure to minimize the contamination of Cu, C, O, and Fe, (2) a HF etching

treatment of the empty fused silica ampoule to reduce the interaction between sample and fused silica ampoule during growth, (3) a Cd reservoir at 820±10 ºC over the melt to consistently grow high resistivity CdZnTe crystals (In dopant concentration of 4 to 6 ppm, atomic) with minimal amount of Te inclusions/precipitates, (4) a mechanical pulsed perturbation to the growth ampoule during the nucleation stage of crystal to promote the yield of single crystal and (5) a cooling schedule of Cd reservoir temperature after the growth process to improve the radial uniformity of electrical properties in the grown crystal. The measured thermal conductivity, electrical conductivity, and Seebeck coefficient of a vapor-grown CdTe and two melt-grown $Cd_{0.8}Zn_{0.2}Te$ crystals between 190ºC and 780ºC have provided an in-depth understanding of the thermal and electrical conduction mechanisms and the prospect of its thermoelectric applications.

Acknowledgements

The author would like to acknowledge the supports of Space Life and Physical Sciences Division, Human Exploration and Operations Mission Directorate, NASA Headquarter and NASA ROSS (Research Opportunities in Space Science) project.

References

[1] P. Rudolph, Prog. Cryst. Growth Charact. 29, 275 (1994).

[2] R. B. James, T. E. Schlesinger, J. Lund, M. Schieber in *Semiconductors and Semimetals*, Vol. 43 (Academic Press, New York, 1997), p. 335

[3] T. E. Schlesinger, J. E. Toney, H. Yoon, E.Y. Lee, B. A. Brunett, L. Franks, R. B. James, Mater. Sci. Eng. 32, 103 (2002).

[4] Stefano Del Sordo, Leonardo Abbene, Ezio Caroli, Anna Maria Mancini, Andrea Zappettini, Pietro Ubertini, Sensors. 9, 3491 (2009).

[5] Csaba Szeles, M. C. Driver, SPIE Proc. Ser., 3446, 1 (1998).

[6] M. Amman, J. S. Lee, P. N. Luke, J. Appl. Phys. 92 3198 (2002).

[7] Csaba Szeles, IEEE Trans. Nucl. Sci. 51, 1242 (2004).

[8] G. A. Carini, A. E. Bolotnikov, G. S. Camarda, G. W. Wright, R. B. James, Appl. Phys. Lett. 88, 143515 (2006).

[9] R. F. Brebrick, *Progress in Solid State Chemistry*, vol.13, Ch. 5, Ed. H. Reiss, (Pergamon Press, Oxford 1967) p.213 p.213.

[10] V. N. Guskov, J. H. Greenberg, M. Fiederle, K.-W. Benz, J. Alloys and Compounds. 371, 118 (2004).

[11] J. H. Greenberg, Prog. Cryst. Growth and Charact. Mater. 47, 196 (2003).

[12] J. H. Greenberg, V. N. Guskov, J. Crystal Growth 289, 552 (2006).

[13] J. Franc, P. Moravec, P. Hlidek, E. Belas, P. Hoschl, R. Grill, Z. Sourek, J. Electron. Mater. 32, 761 (2003).

[14] H. Chen, S. A. Awadalla, K. Iniewski, P. H. Lu, F. Harris, J. Mackenzie, T. Hasanen, W. Chen, R. Redden, G. Bindley, Irfan Kuvvetli, Carl Budtz-Jørgensen, P. Luke, M. Amman, J.

S. Lee, A. E. Bolotnikov, G. S. Camarda, Y. Cui, A. Hossain, R. B. James, J. Appl. Phys. 103, 014903 (2008).

[15] P. Fougeres, P. Siffert, M. Hageali, J. M. Koebel, R. Regal, Nucl. Instr. Methods in Phys. Research. A428, 38 (1999).

[16] Guoqiang Li, Wanqi Jie, Hui Hua, Zhi Gu, Prog. Cryst. Growth and Charact. Mater. 46, 85 (2003).

[17] Rei Fang and R. F. Brebrick, J. Phys. Chem. Solids. 57, 443 (1996).

[18] Ching-Hua Su, J. Crystal Growth. 281, 577 (2005).

[19] T.-C. Yu, R. F. Brebrick, J. Phase Equilibria. 13, 476 (1992).

[20] J. Franc, R. Grill, P. Hlidek, E. Belas, L. Turjanska, P. Hoschl, I. Turkevych, A. L. Toth, P. Moravec, H. Sitter, Semicond. Sci. Technol. 16, 514 (2001).

[21] T. Asahi, O. Oda, Y. Taniguchi, A. Koyama, J. Crystal Growth. 161, 20 (1996) .

[22] A. Koyama, A. Hichiwa, R. Hirano, J. Electron. Mater. 28, 587 (1999).

[23] C. Szeles, E. Eissler, D.J. Reese, S.E. Cameron, SPIE Conf. Proc. 3768, 98 (1999).

[24] C. Szeles, S.E. Cameron, J.-O. Ndap, W.C. Chalmers, IEEE Trans. Nucl. Sci. 49, 2535 (2002).

[25] R. F. Brebrick, Rei Fang, J. Phys. Chem. Solids. 57, 451 (1996).

[26] R. F. Brebrick, private communication.

[27] Wenbin Sang, Yongbiao Qian, Weiming Shi, Linjun Wang, Ju Yang, Donghua Liu, J. Crystal Growth. 214/215, 30 (2000).

[28] Ching-Hua Su, S. L. Lehoczky, F. R. Szofran, J. Appl. Phys. 60, 3777 (1986).

[29] M. Fiederlea, T. Duffar, J. P. Garandet, V. Babentsov, A. Fauler, K. W. Benz, P. Dusserre, V. Corregidor, E. Dieguez, P. Delaye, G. Roosen, V. Chevrier, J. C. Launay, J. Crystal Growth. 267, 429 (2004).

[30] Ching-Hua Su, Cryst. Res. Technol. 1900208 (2020).

[31] Ching-Hua Su, S. L. Lehoczky, F. R. Szofran, J. Crystal Growth. 86, 87 (1988).

[32] Ching-Hua Su, J. Crystal Growth. 410, 35 (2015).

[33] E. Belas, R. Grill, J. Franc, L. Turjanska, I. Turkevych, P. Moravec, P. Hoschl, J. Electronic Mater. 32, 752 (2003).

[34] J. Steininger, A. J. Strauss, R. F. Brebrick, J. Electrochem. Soc. 117, 1305 (1970).

[35] A. Haloui, Y. Feutelais, B. Legendre, J. Alloys and Compounds. 260, 179 (1997).

[36] L. Shcherbak, P. Feychuk, Yu. Plevachuk, Ch. Dong, O. Kopach, O. Panchuk, P. Siffert, J. Alloys and Compounds. 371, 186 (2004).

[37] L. Shcherbak, P. Feichouk, O. Panchouk, J. Crystal Growth. 161, 16 (1996).

[38] L. Shcherbak, J. Crystal Growth. 197, 397 (1999).

[39] Ching-Hua Su and S. L. Lehoczky J. Crystal Growth. 319, 4 (2011).

[40] Z. Burshtein, H. N. Jayatirtha, A. Burger, J. F. Butler, B. Apotovsky, F. P. Doty, Appl. Phys. Lett. 63, 102 (1993).

[41] P. Rudolph, A. Engel, I. Schentke, A. Grochocki, J. Crystal Growth. 147, 279 (1995).

[42] Ching-Hua Su, AIP Advances. 5, 057118 (2015).

[43] K. Chattopadhyay, S. Feth, H. Chen, A. Burger, Ching-Hua Su, J. Crystal Growth, 191. 377 (1998).

[44] Ching-Hua Su, Yi-Gao Sha, S. L. Lehoczky, Hao-Chieh Liu, Rei Fang, R. F. Brebrick, J. Crystal Growth. 183, 519 (1998).

[45] L. M. Clark, R. E. Taylor, J. Appl. Phys. 46, 714 (1975).

[46] D. J. Williams, *Properties of Narrow Gap Cadmium-based Compounds*, edited by P. Capper, emis Datareviews series, (INSPECT publication, 1994) p.399.

[47] R. N. Bhargava, *Properties of Wide Bandgap II-VI Semiconductors*, edited by R. Bhargava, emis Datareviews series, (INSPECT publication, 1997) p.27.

[48] K. C. Mills, *Thermodynamic Data for Inorganic Sulphides, Selenides and Tellurides*, (Butterworths, London 1974).

[49] I. Barin, O. Knacke, O. Kubaschewski, *Thermochemical Properties of Inorganic Substances (Supplement* Springer-Verlag 1977).

[50] S. Sen, W. H. Konkel, S. J. Tighe, L. G. Bland, S. R. Sharma, R. E. Taylor, J. Crystal Growth. 86. 111 (1988).

[51] P. Hoschl, E. Belas, L. Tujanska, R. Grill, J. Franc, R. Fesh, P. Moravec, J. Crystal Growth. 220, 444 (2000).

[52] Ching-Hua Su, J. Appl. Phys. 103, 084903 (2008).

[53] S. M. Johnson, S. Sen, W. H. Konkel, M. H. Kalisher, J. Vac. Sci. Technol. B9, 1987 (1991).

[54] F. T. J. Smith, Met. Trans. 1, 617 (1970).